Publication Year	2019
Acceptance in OA@INAF	2021-04-16T17:04:48Z
Title	Cosmological constraints on post-Newtonian parameters in effectively massless scalar-tensor theories of gravity
Authors	Rossi, Massimo; Ballardini, Mario; BRAGLIA, MATTEO; FINELLI, FABIO; PAOLETTI, DANIELA; et al.
DOI	10.1103/PhysRevD.100.103524
Handle	http://hdl.handle.net/20.500.12386/30789
Journal	PHYSICAL REVIEW D
Number	100

Cosmological constraints on post-Newtonian parameters in effectively massless scalar-tensor theories of gravity

Massimo Rossi,[1,*] Mario Ballardini,[2,3,1,†] Matteo Braglia,[4,1,5,‡] Fabio Finelli,[1,5,§] Daniela Paoletti,[1,5,‖] Alexei A. Starobinsky,[6,7,¶] and Caterina Umiltà[8,**]

[1]*INAF/OAS Bologna, via Gobetti 101, I-40129 Bologna, Italy*
[2]*Dipartimento di Fisica e Astronomia, Alma Mater Studiorum Universitá di Bologna, Via Gobetti, 93/2, I-40129 Bologna, Italy*
[3]*Department of Physics and Astronomy, University of the Western Cape, Cape Town 7535, South Africa*
[4]*Dipartimento di Fisica e Astronomia, Alma Mater Studiorum, Università degli Studi di Bologna, via Gobetti 101, I-40129 Bologna, Italy*
[5]*INFN, Sezione di Bologna, Via Irnerio 46, I-40127 Bologna, Italy*
[6]*Landau Institute for Theoretical Physics, 119334 Moscow, Russia*
[7]*Bogolyubov Laboratory of Theoretical Physics, Joint Institute for Nuclear Research, Dubna 141980, Russia*
[8]*Department of Physics, University of Cincinnati, 345 Clifton Court, Cincinnati, Ohio 45221, USA*

(Received 27 June 2019; published 18 November 2019)

We study the cosmological constraints on the variation of Newton's constant and on post-Newtonian parameters for simple models of the scalar-tensor theory of gravity beyond the extended Jordan-Brans-Dicke theory. We restrict ourselves to an effectively massless scalar field with a potential $V \propto F^2$, where $F(\sigma) = N_{\rm pl}^2 + \xi\sigma^2$ is the coupling to the Ricci scalar considered. We derive the theoretical predictions for cosmic microwave background anisotropies and matter power spectra by requiring that the effective gravitational strength at present is compatible with the one measured in a Cavendish-like experiment and by assuming an adiabatic initial condition for scalar fluctuations. When comparing these models with Planck 2015 and a compilation of baryonic acoustic oscillations data, all these models accommodate a marginalized value for H_0 higher than in ΛCDM. We find no evidence for a statistically significant deviation from Einstein's general relativity. We find $\xi < 0.064$ ($|\xi| < 0.011$) at 95% CL for $\xi > 0$ (for $\xi < 0$, $\xi \neq -1/6$). In terms of post-Newtonian parameters, we find $0.995 < \gamma_{\rm PN} < 1$ and $0.99987 < \beta_{\rm PN} < 1$ ($0.997 < \gamma_{\rm PN} < 1$ and $1 < \beta_{\rm PN} < 1.000011$) for $\xi > 0$ (for $\xi < 0$). For the particular case of the conformal coupling, i.e., $\xi = -1/6$, we find constraints on the post-Newtonian parameters of similar precision to those within the Solar System.

DOI: 10.1103/PhysRevD.100.103524

I. INTRODUCTION

The astrophysical and cosmic tests for the change of the fundamental physical constants are improving thanks to the increasing precision of observations [1,2]. In most of the cases these tests cannot compete with the precision which can be achieved in laboratories, but they can probe lengths and/or timescales otherwise unaccessible on ground. There are however exceptions: For instance, current cosmological data can constrain the time variation of the Newtonian constant at the same level of experiments within the Solar System such as Lunar Laser ranging [3,4].

As far as cosmological tests are concerned, one workhorse model to test deviations from general relativity (GR) is the extended Jordan-Brans-Dicke (eJBD) [5,6] theory, which has been extensively studied [3,4,7–12]. The eJBD is perhaps the simplest extension of GR within the more general Horndeski theory [13]:

$$S = \int \mathrm{d}^4x\sqrt{-g}\Big[G_2(\sigma,\chi) + G_3(\sigma,\chi)\Box\sigma + G_4(\sigma,\chi)R - 2G_{4,\chi}(\sigma,\chi)(\Box\sigma^2 - \sigma^{;\mu\nu}\sigma_{;\mu\nu}) + G_5(\sigma,\chi)G_{\mu\nu}\sigma^{;\mu\nu} + \frac{1}{3}G_{5,\sigma}(\sigma,\chi)(\Box\sigma^3 - 3\sigma_{;\mu\nu}\sigma^{;\mu\nu}\Box\sigma + 2\sigma_{;\mu\nu}\sigma^{;\nu\rho}\sigma^{;\mu}{}_{;\rho}) + \mathcal{L}_m\Big], \tag{1}$$

*rossi.massim@gmail.com
†mario.ballardini@inaf.it
‡matteo.braglia2@unibo.it
§fabio.finelli@inaf.it
‖daniela.paoletti@inaf.it
¶alstar@landau.ac.ru
**umiltca@ucmail.uc.edu

 © 2019 American Physical Society

where $\chi = -g^{\mu\nu}\partial_\mu\sigma\partial_\nu\sigma$, ";" denotes the covariant derivative, R is the Ricci scalar, $G_{\mu\nu} = R_{\mu\nu} - g_{\mu\nu}R/2$, and $\mathcal{L}_m$ is the density Lagrangian for the rest of the matter. The eJBD theory corresponds to $G_3 = G_5 = 0$, $G_2 = \omega_{\rm BD}\chi/\sigma - V(\sigma)$, $G_4 = \sigma$ [in the equivalent induced gravity (IG) formulation with a standard kinetic term, the last two conditions become $G_2 = \chi/2 - V(\sigma)$, $G_4 = \xi\sigma^2/2$ with $\xi = 1/(4\omega_{\rm BD})$].

Cosmology puts severe tests on eJBD theories. The constraints from Planck 2015 and a compilation of baryon acoustic oscillations (BAO) data lead to a 95% CL upper bound $\xi < 0.00075$, weakly dependent on the index for a power-law potential [4] (see [3] for the Planck 2013 constraints obtained with the same methodology). In terms of the first post-Newtonian parameter $\gamma_{\rm PN} = (1+\omega_{\rm BD})/(2+\omega_{\rm BD}) = (1+4\xi)/(1+8\xi)$, the above 95% CL constraint reads as $|\gamma_{\rm PN} - 1| < 0.003$ [4]. With the same data, a 95% CL bound is obtained on the relative time variation of the effective Newton's constant $10^{13}|\dot{G}_{\rm eff}/G_{\rm eff}| \lesssim 6\times10^{-3}H_0$ at 95% CL with an index for a power-law potential in the range [0, 8]. The combination of future measurements of CMB anisotropies in temperature, polarization, and lensing with Euclid-like (galaxy clustering and weak lensing) data can lead to constraints on $\gamma_{\rm PN}$ at a slightly larger level than the current Solar System constraints [14] (see also [15] for forecasts for different experiments with different assumptions).

However, theoretical priors can play an important role in the derivation of the cosmological constraints and need to be taken into account in the comparison with other astrophysical or laboratory tests. Indeed, for eJBD theories only the first post-Newtonian parameter $\gamma_{\rm PN}$ is nonzero and fully encodes the deviations from GR, with the second post-Newtonian parameter $\beta_{\rm PN} \propto {\rm d}\gamma_{\rm PN}/{\rm d}\sigma$. In this paper we go beyond the working assumption of $\beta_{\rm PN} = 0$ implicit within eJBD theories. For this purpose we therefore consider nonminimally coupled (NMC) scalar fields with $2G_4 = N_{\rm pl}^2 + \xi\sigma^2$ as a minimal generalization of the eJBD theories. NMC scalar fields with this type of coupling are also known as extended quintessence models in the context of dark energy (DE) [16–20]. As for eJBD, NMC scalar fields are also within the class of Horndeski theories consistent with the constraints on the velocity of propagation of gravitational waves [21–23], which followed the observation of GW170817 and its electromagnetic counterpart [24] (see also [25,26]).

The outline of this paper is as follows. In Sec. II we discuss the background dynamics and the post-Newtonian parameters $\gamma_{\rm PN}$ and $\beta_{\rm PN}$ for this class of scalar-tensor theories. We study the evolution of linear fluctuations in Sec. III. We show the dependence on ξ of the CMB anisotropies power spectra in temperature and polarization in Sec. IV. We present the Planck and BAO constraints on these models in Sec. V. We conclude in Sec. VI. The initial conditions for background and cosmological fluctuations are collected in the Appendix.

II. DARK ENERGY AS AN EFFECTIVELY MASSLESS SCALAR FIELD NONMINIMALLY COUPLED TO GRAVITY

We study the restriction of the Horndeski action (1) to a standard kinetic term and $G_3 = G_5 = 0$. We also assume

$$2G_4 \equiv F(\sigma) = N_{\rm pl}^2 + \xi\sigma^2, \tag{2}$$

where ξ is the coupling to the Ricci scalar which is commonly used in extended quintessence [16–20]. For simplicity, we denote by a tilde the quantities normalized to $M_{\rm pl} \equiv 1/\sqrt{8\pi G}$, where $G = 6.67\times10^{-8}$ cm^3 g^{-1} s^{-2} is the gravitational constant measured in a Cavendish-like experiment. We also introduce the notation $\tilde{N}_{\rm pl} \equiv 1 \mp \Delta\tilde{N}_{\rm pl}$ for $\xi \gtrless 0$.

The field equations are obtained by varying the action with respect to the metric:

$$G_{\mu\nu} = \frac{1}{F(\sigma)}\left[T_{\mu\nu} + \partial_\mu\sigma\partial_\nu\sigma - \frac{1}{2}g_{\mu\nu}\partial^\rho\sigma\partial_\rho\sigma - g_{\mu\nu}V(\sigma) + (\nabla_\mu\nabla_\nu - g_{\mu\nu}\Box)F(\sigma)\right]. \tag{3}$$

We obtain the Einstein trace equation

$$R = \frac{1}{F}[-T + \partial_\mu\sigma\partial^\mu\sigma + 4V + 3\Box F], \tag{4}$$

where T is the trace of the energy-momentum tensor. The Klein-Gordon (KG) equation can be obtained by varying the action with respect to the scalar field:

$$-\Box\sigma - \frac{1}{2}F_{,\sigma}R + V_{,\sigma} = 0, \tag{5}$$

and substituting the Einstein trace equation, one obtains

$$-\Box\sigma\left(1 + \frac{3}{2}\frac{F_{,\sigma}^2}{F}\right) + V_{,\sigma} - 2\frac{VF_{,\sigma}}{F} + \frac{F_{,\sigma}}{2F}[T - \partial_\mu\sigma\partial^\mu\sigma(1 + 3F_{,\sigma\sigma})] = 0. \tag{6}$$

In this paper, we do not consider a quintessence-like inverse power-law potential (see for instance [16–18,20]), but we restrict ourselves to a potential of the type $V \propto F^2$ in which the scalar field is effectively massless. This case generalizes the broken scale invariant case [27–29] to the NMC scalar field and is a particular case of the class of models with $V \propto F^M$ admitting scaling solutions [19]. Note that although for the form of $F(\sigma)$ used in the paper and for large values of σ, this potential looks similar to that in the

Higgs inflationary model [30], in fact it is crucially different since it is exactly flat in the Einstein frame[1] in the absence of other matter and cannot support a metastable inflationary stage in the early Universe. In contrast, this model may be used for the description of dark energy in the present Universe.

A. Background cosmology

We consider cosmic time and a flat FLRW metric for which the unperturbed cosmological spacetime metric is given by

$$ds^2 = -dt^2 + a(t)^2 dx_i dx^i. \tag{7}$$

The Friedmann and the KG equations are then given by

$$3H^2F = \rho + \frac{\dot{\sigma}^2}{2} + V(\sigma) - 3H\dot{F} = \rho + \rho_\sigma, \tag{8}$$

$$-2\dot{H}F = \rho + p + \dot{\sigma}^2 + \ddot{F} - H\dot{F} = (\rho + p) + \rho_\sigma + p_\sigma, \tag{9}$$

$$\ddot{\sigma} = -3H\dot{\sigma} + \frac{\xi\sigma}{F + 6\xi^2\sigma^2}\left[\rho_m + 4V - \frac{FV_{,\sigma}}{\xi\sigma} - (1 + 6\xi)\dot{\sigma}^2\right]. \tag{10}$$

In Fig. 1 the evolution of the scalar field σ is shown for different values of ξ for both positive and negative values of the coupling. The natural initial conditions for the background displayed in the Appendix neglect the decaying mode, which would rapidly dissipate but would destroy the Universe isotropy at sufficiently early times otherwise (see for instance [29]). With this natural assumption the scalar field is nearly at rest deep in the radiation era, whereas it grows (decreases) for positive (negative) couplings during the matter era and it reaches a constant value at recent times. During the matter dominated era in the regime $\xi\sigma^2 \ll N_{\rm pl}^2$ (which is the only one allowed by observations, see Sec. V), the evolution of the scalar field can be approximated as $\sigma \sim \sigma_i[1 + 2\xi(\ln a + 8)]$, with σ_i being the initial value of the scalar field in the radiation era. In the bottom panel, we show the evolution of the scalar field for the conformal coupling (CC) case with $\xi = -1/6$ for different values of $N_{\rm pl}$. In this case the field is always sub-Planckian for $\Delta\tilde{N}_{\rm pl} \lesssim 0.0005$.

The above equations lead to the straightforward associations:

[1]Although our work is based in the original Jordan frame, it is also useful to think about this class of theories in the dual Einstein frame where $\hat{g}_{\mu\nu} \propto F g_{\mu\nu}, \hat{V} = V/F^2$.

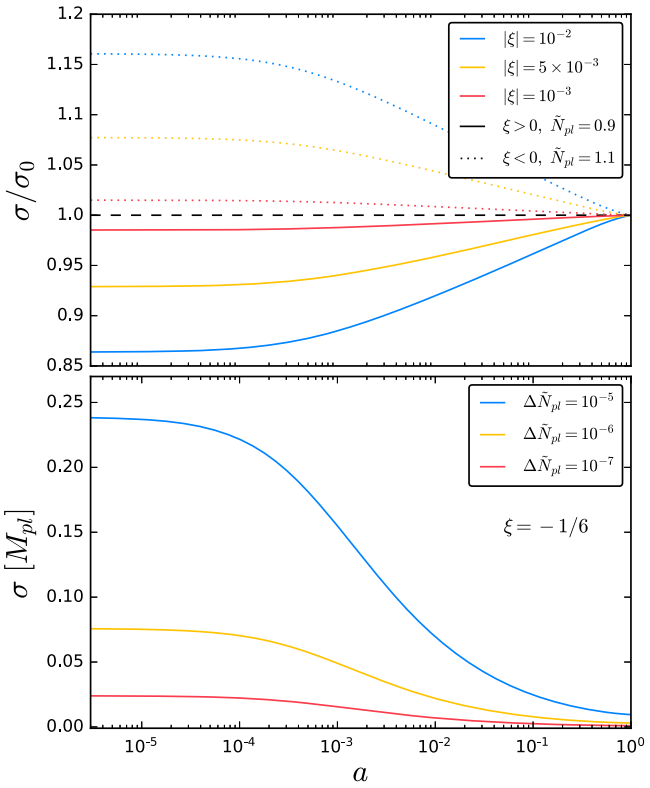

FIG. 1. Top panel: Relative evolution of σ for different values of ξ. Bottom panel: Evolution of σ for different values of $N_{\rm pl}$ for the CC case, i.e., $\xi = -1/6$.

$$\rho_\sigma = \frac{\dot{\sigma}^2}{2} + V(\sigma) - 3H\dot{F} = \frac{\dot{\sigma}^2}{2} + V(\sigma) - 6H\xi\sigma\dot{\sigma}, \tag{11}$$

$$p_\sigma = \frac{\dot{\sigma}^2}{2}\left[\frac{F(1 + 4\xi) + 2\xi^2\sigma^2}{F + 6\xi^2\sigma^2}\right] - 2H\xi\sigma\dot{\sigma} + \frac{2\xi^2\sigma^2}{F + 6\xi^2\sigma^2}\left(\rho_m + 4V - \frac{FV_{,\sigma}}{\xi\sigma}\right) - V, \tag{12}$$

where in the equation for p_σ we have explicitly substituted the KG equation. We can recover an expression for the DE density parameter dividing ρ_σ for the quantity $3H^2F$, which represents the critical density.

Alternatively, it is also convenient to define new density parameters in a framework which mimics Einstein gravity at present and to satisfy the conservation law $\dot{\rho}_{\rm DE} + 3H(\rho_{\rm DE} + p_{\rm DE}) = 0$ [31,32]:

$$\rho_{\rm DE} = \frac{F_0}{F}\rho_\sigma + (\rho_m + \rho_r)\left(\frac{F_0}{F} - 1\right), \tag{13}$$

$$p_{\rm DE} = \frac{F_0}{F}p_\sigma + p_r\left(\frac{F_0}{F} - 1\right). \tag{14}$$

The effective parameter of state for DE can be defined as $w_{\rm DE} \equiv p_{\rm DE}/\rho_{\rm DE}$.

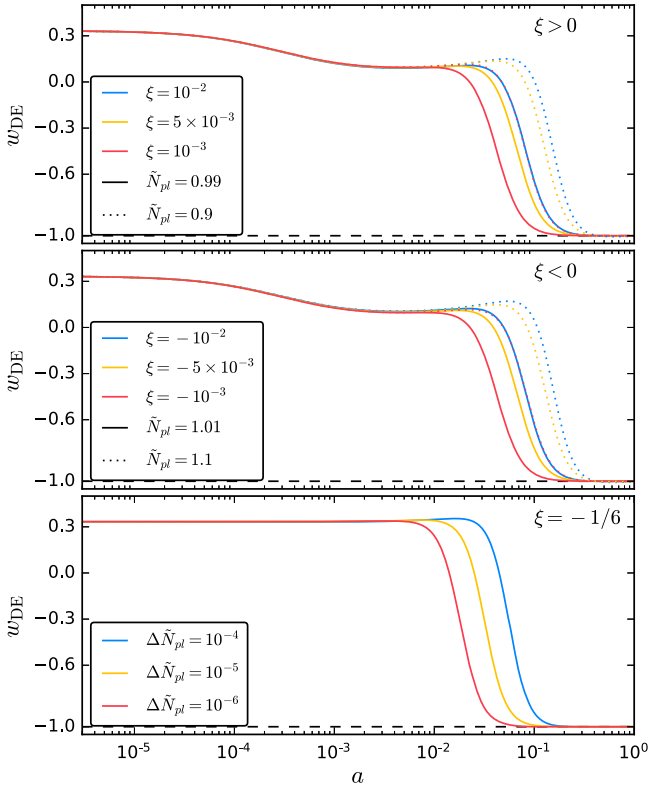

FIG. 2. Evolution of $w_{\rm DE}$ for different values of $N_{\rm pl}$ and ξ. We plot the effective parameter of state for DE for $\xi > 0$ in the upper panel, $\xi < 0$ in the central panel, and the CC case $\xi = -1/6$ in the bottom panel.

In Fig. 2 the evolution of this effective parameter of state is shown for different values of the parameters $N_{\rm pl}$ and ξ. In all cases the parameter of state $w_{\rm DE}$ mimics $1/3$ (-1) in the relativistic era (at late times): This behavior can be easily understood from Eqs. (13) and (14) when ρ_r $[V(\sigma)]$ dominates over the energy densities of the other components. The behavior of $w_{\rm DE}$ at the onset of the matter dominated era is instead model dependent: For $\xi \neq -1/6$, we see that $w_{\rm DE} > 0$ from the upper two panels in Fig. 2, whereas for $\xi = -1/6$ we obtain $w_{\rm DE} \sim 1/3$ when $\sigma_0 \ll \sigma$. The absence of an intermediate phase of a matter dominated era for $\xi = -1/6$ is also clear in the initial conditions for the scale factor reported in the Appendix. It can be seen from Fig. 2 that there is no phantom behavior of the effective DE component at small redshifts, in contrast to the more general scalar-tensor DE models studied in [32]. Indeed, a phantom behavior with $w_{\rm DE} < -1$ [32] is barely visible in the transient regime from the tracking value to $w_{\rm DE} \approx -1$ because of the small coupling ξ considered in Fig. 2, and it cannot occur in the stable accelerating regime for these models with $V(\sigma) \propto F^2(\sigma)$.

In Figs. 3–5, we show the evolution of the density parameters Ω_i, corresponding to an Einstein gravity system with a Newton's constant given by the current value of the scalar field today, $G_N = 1/(8\pi F_0)$ [31] (also used in [3,33]), for $\xi > 0$, $\xi < 0$, and $\xi = -1/6$, respectively.

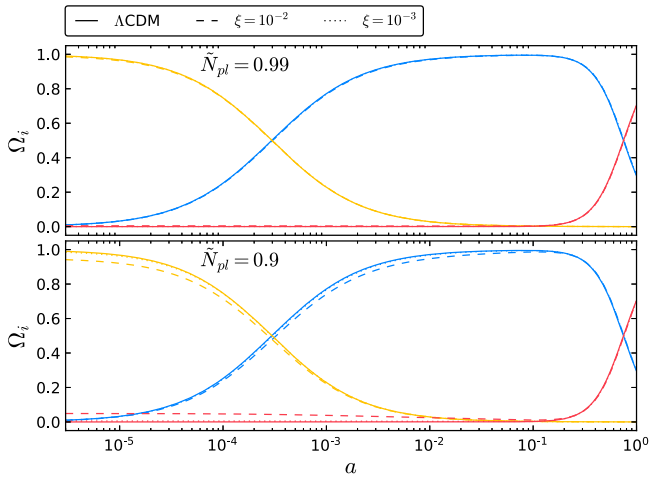

FIG. 3. Evolution of the density parameters Ω_i: radiation in yellow, matter in blue, and effective DE in red. We plot $\tilde{N}_{\rm pl} = 1$ ($\tilde{N}_{\rm pl} = 0.9$) for $\xi = 10^{-2}, 10^{-3}$ in the top (bottom) panel.

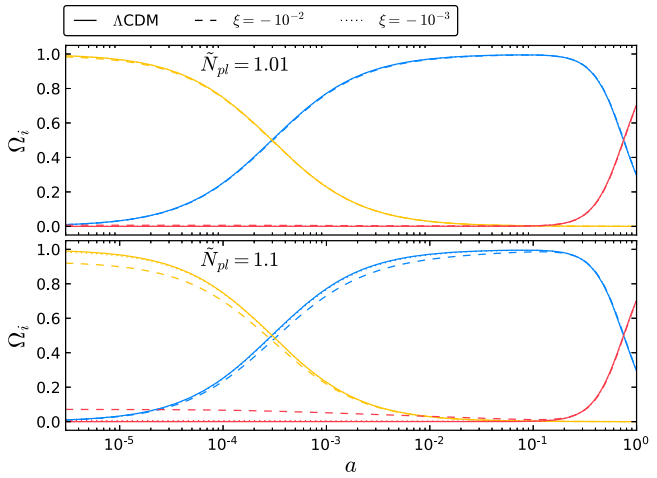

FIG. 4. Evolution of the density parameters Ω_i: radiation in yellow, matter in blue, and effective DE in red. We plot $\tilde{N}_{\rm pl} = 1.01$ ($\tilde{N}_{\rm pl} = 1.1$) for $\xi = -10^{-2}, -10^{-3}$ in the top (bottom) panel.

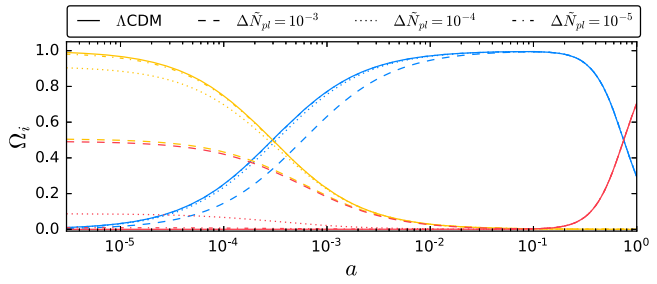

FIG. 5. Evolution of the density parameters Ω_i: radiation in yellow, matter in blue, and effective DE in red. We plot the CC case $\xi = -1/6$ for $\Delta\tilde{N}_{\rm pl} = 10^{-3}, 10^{-4}, 10^{-5}$.

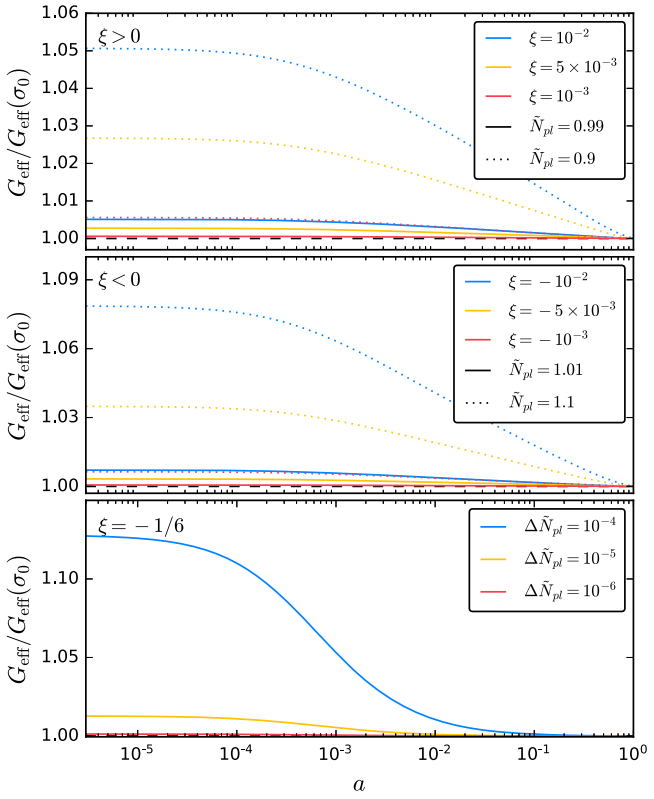

FIG. 6. Evolution of the effective gravitational constant $G_{\rm eff}$ relative to its value today for different values of $N_{\rm pl}$ and ξ. From top to bottom, the cases with $\xi > 0$, $\xi < 0$, and $\xi = -1/6$ are displayed, respectively.

B. Boundary conditions for the scalar field

As boundary conditions we impose that the effective Newton constant at present is compatible with the Cavendish-like experiments. The effective gravitational constant for NMC scalar fields is given by [31]

$$G_{\rm eff} = \frac{1}{8\pi F}\left(\frac{2F + 4F_{,\sigma}^2}{2F + 3F_{,\sigma}^2}\right). \tag{15}$$

Figure 6 shows the evolution of the relative effective gravitational constant (15). We can see that the effective gravitational constant decreases in time for all the choices of both $N_{\rm pl}$ and ξ.

We can distinguish three different cases beyond GR:

(i) $\tilde{N}_{\rm pl} \to 0$, which is the IG case. This leads to

$$\tilde{\sigma}_0^2 = \frac{1}{\xi}\frac{1+8\xi}{1+6\xi}, \tag{16}$$

which is the same result as obtained in [3].

(ii) $\xi \to -1/6$, which is the CC. In this particular case the polynomial equation (15) in σ_0 is quadratic, and we have

$$\tilde{\sigma}_0^2 = \frac{18\tilde{N}_{\rm pl}^2(\tilde{N}_{\rm pl}^2 - 1)}{1 + 3\tilde{N}_{\rm pl}^2}. \tag{17}$$

(iii) A general NMC case for $\xi \neq -1/6$:

$$\tilde{\sigma}_0^2 = \frac{1 - 2\tilde{N}_{\rm pl}^2 + 2\xi(4 - 3\tilde{N}_{\rm pl}^2)}{2\xi(1+6\xi)} \pm \frac{\sqrt{1 - 4\xi(5\tilde{N}_{\rm pl}^2 - 4) + 4\xi^2(3\tilde{N}_{\rm pl}^2 - 4)^2}}{2\xi(1+6\xi)}. \tag{18}$$

By requiring $\tilde{\sigma}^2 \geq 0$ and $F \geq 0$, we obtain conditions on the two parameters $\tilde{N}_{\rm pl}$ and ξ for the physical solution:

$$\tilde{N}_{\rm pl} < 1 \quad \text{for } \xi > 0, \tag{19}$$

$$\tilde{N}_{\rm pl} > 1 \quad \text{for } \xi < 0. \tag{20}$$

C. Comparison with general relativity

The deviations from GR for a theory of gravitation are described by the so-called post-Newtonian parameters.

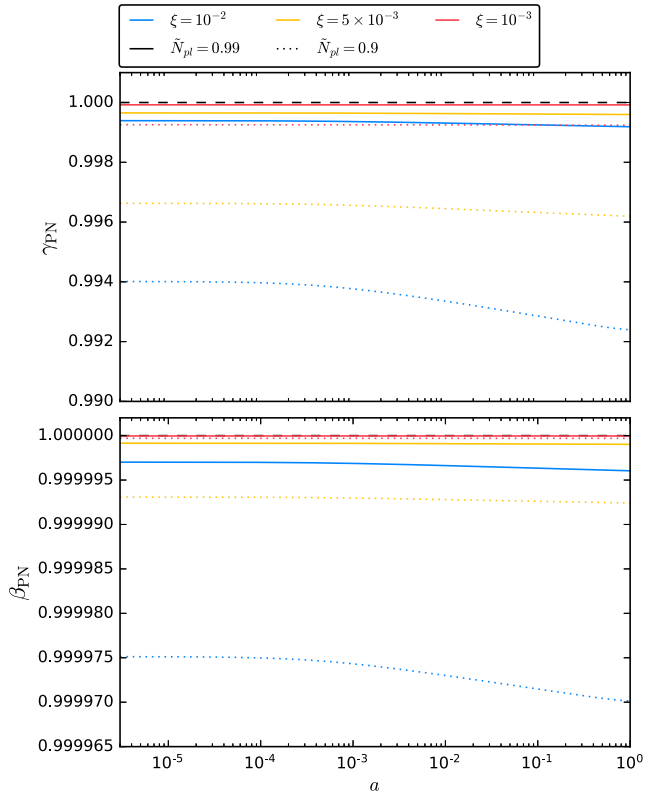

FIG. 7. Evolution of the post-Newtonian parameters $\gamma_{\rm PN}$ and $\beta_{\rm PN}$ for different values of $N_{\rm pl}$ and ξ. We show the case with $\xi > 0$.

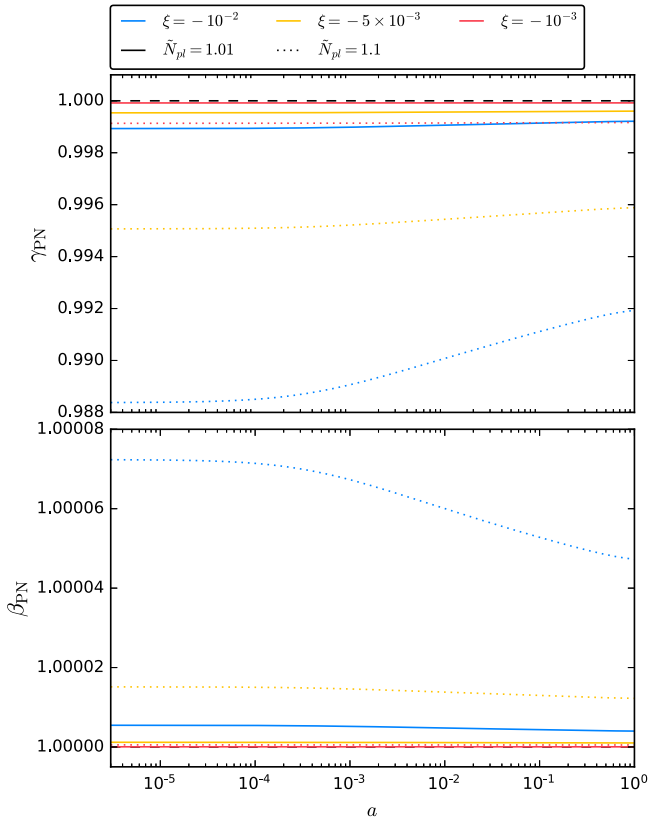

FIG. 8. Evolution of the post-Newtonian parameters $\gamma_{\rm PN}$ and $\beta_{\rm PN}$ for different values of $N_{\rm pl}$ and ξ. We show the NMC case with $\xi > 0$.

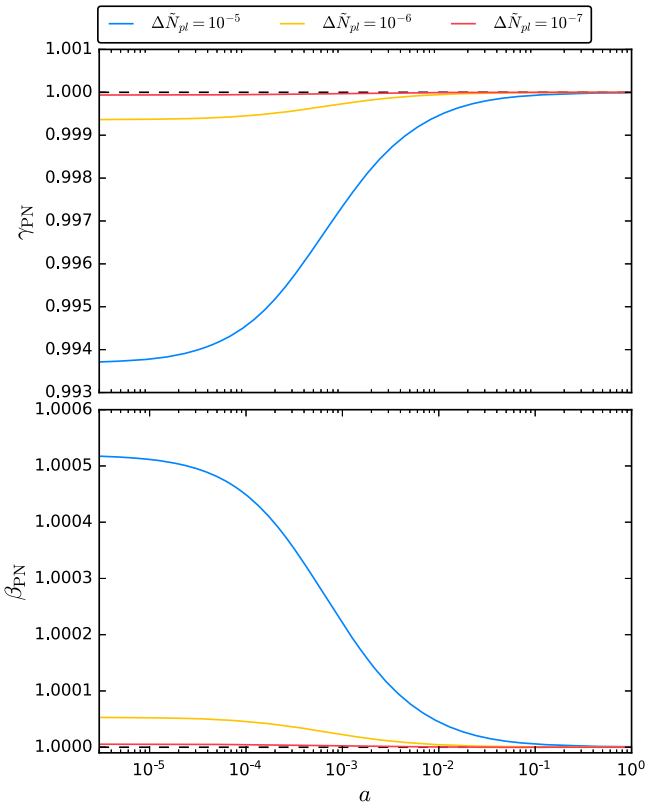

FIG. 9. Evolution of the post-Newtonian parameters $\gamma_{\rm PN}$ and $\beta_{\rm PN}$ for different values of $N_{\rm pl}$. We show the NMC case $\xi = -1/6$, i.e., the CC case.

For NMC scalar fields only the parameters $\gamma_{\rm PN}$ and $\beta_{\rm PN}$ differ from GR predictions, for which they both equal unity. In terms of these parameters, the line element can be expressed as

$$ds^2 = -(1 + 2\Phi - 2\beta_{\rm PN}\Phi^2)dt^2 + (1 - 2\gamma_{\rm PN}\Phi)dx_i dx^i. \tag{21}$$

These parameters are given within NMC scalar fields by the following equations [31]:

$$\gamma_{\rm PN} = 1 - \frac{F_{,\sigma}^2}{F + 2F_{,\sigma}^2}, \tag{22}$$

$$\beta_{\rm PN} = 1 + \frac{FF_{,\sigma}}{8F + 12F_{,\sigma}^2}\frac{d\gamma_{\rm PN}}{d\sigma}. \tag{23}$$

We have $\gamma_{\rm PN} \leq 1$ and $\beta_{\rm PN} \leq 1$ for $\xi > 0$, whereas $\gamma_{\rm PN} \leq 1$ and $\beta_{\rm PN} \geq 1$ for $\xi < 0$.

In Figs. 7–9, we show the evolution of these parameters for different values of $N_{\rm pl}$ and ξ. It is interesting to note how, in the CC case, $\gamma_{\rm PN}$ and $\beta_{\rm PN}$ approach the GR value more rapidly than for $\xi \neq -1/6$.

III. LINEAR PERTURBATIONS

We study linear fluctuations around the FRW metric in the synchronous gauge:

$$ds^2 = a(\tau)^2[-d\tau^2 + (\delta_{ij} + h_{ij})dx^i dx^j], \tag{24}$$

where τ is the conformal time and h_{ij} include both the scalar (h_{ij}^S) and the tensor (h_{ij}^T) part. We follow the conventions of Ref. [34] for scalar metric perturbations h_{ij} and scalar field perturbation $\delta\sigma$:

$$h_{ij}^S = \int d^3k e^{i\vec{k}\cdot\vec{x}}\left[\hat{k}_i\hat{k}_j h(\vec{k},\tau) + \left(\hat{k}_i\hat{k}_j - \frac{1}{3}\delta_{ij}\right)\eta(\vec{k},\tau)\right], \tag{25}$$

$$\delta\sigma = \int d^3k e^{i\vec{k}\cdot\vec{x}}\delta\sigma(\vec{k},\tau). \tag{26}$$

In Fig. 10, we show the evolution of the scalar field perturbation $\delta\sigma$ at $k = 0.05$ Mpc^{-1} for different values of $N_{\rm pl}$ and ξ.

The modified Einstein equations in Eq. (3) at first order for scalar perturbations are

$$\frac{k^2}{a^2}\eta - \frac{1}{2}H\dot{h} = -\frac{1}{2F}\left[\delta\rho + \dot{\sigma}\delta\dot{\sigma} + V_{,\sigma}\delta\sigma - \frac{F_{,\sigma}}{F}\left(\rho + \frac{\dot{\sigma}^2}{2} + V - 3H\dot{F}\right)\delta\sigma\right], \tag{27}$$

$$\frac{k^2}{a^2}\dot{\eta} = \frac{1}{2F}\left[\sum_i (\rho_i + p_i)\theta_i + k^2(\dot{\sigma}\delta\sigma + \delta\dot{F} - H\delta F)\right], \tag{28}$$

$$\ddot{h} + 3H\dot{h} - 2\frac{k^2}{a^2}\eta = -\frac{3}{F}\left[p + \dot{\sigma}\delta\dot{\sigma} - V_{,\sigma}\delta\sigma - \frac{F_{,\sigma}}{F}\left(p + \frac{\dot{\sigma}^2}{2} - V + \ddot{F} + 2H\dot{F}\right)\delta\sigma + \frac{2}{3}\frac{k^2}{a^2}\delta F + \delta\ddot{F} + 2H\delta\dot{F} + \frac{1}{3}\dot{h}\,\dot{F}\right], \tag{29}$$

$$\ddot{h} + 6\ddot{\eta} + 3H(\dot{h} + 6\dot{\eta}) - 2\frac{k^2}{a^2}\eta = -\frac{3}{F}\left[\sum_i (\rho_i + p_i)\sigma_i + \frac{2}{3}\frac{k^2}{a^2}\delta F + \frac{\dot{F}}{3}(\dot{h} + 6\dot{\eta})\right], \tag{30}$$

where all perturbations are considered in the Fourier configuration. The quantities θ_i and σ_i represent the velocity potential and the anisotropic stress, respectively. It can be seen from the last of these equations that the coupling function also acts as a source for the anisotropic stress.

The perturbed Klein-Gordon equation is

$$\begin{aligned}\delta\ddot{\sigma} = &-\delta\dot{\sigma}\left[3H + \frac{2(1+6\xi)\xi\sigma\dot{\sigma}}{F + 6\xi^2\sigma^2}\right] - \delta\sigma\left\{\frac{k^2}{a^2} + \frac{FV_{,\sigma,\sigma}}{F + 6\xi^2\sigma^2} - \frac{2\xi\sigma V_{,\sigma}}{F + 6\xi^2\sigma^2}\left[1 + \frac{F(1+6\xi)}{F + 6\xi^2\sigma^2}\right]\right.\\ &\left. + \frac{\xi}{F + 6\xi^2\sigma^2}\left[1 - \frac{2(1+6\xi)\xi\sigma^2}{F + 6\xi^2\sigma^2}\right][(1+6\xi)\dot{\sigma}^2 - 4V + (3p - \rho)]\right\} - \frac{(3\delta p - \delta\rho)\xi\sigma}{F + 6\xi^2\sigma^2} - \frac{1}{2}\dot{h}\,\dot{\sigma}\,.\end{aligned} \tag{31}$$

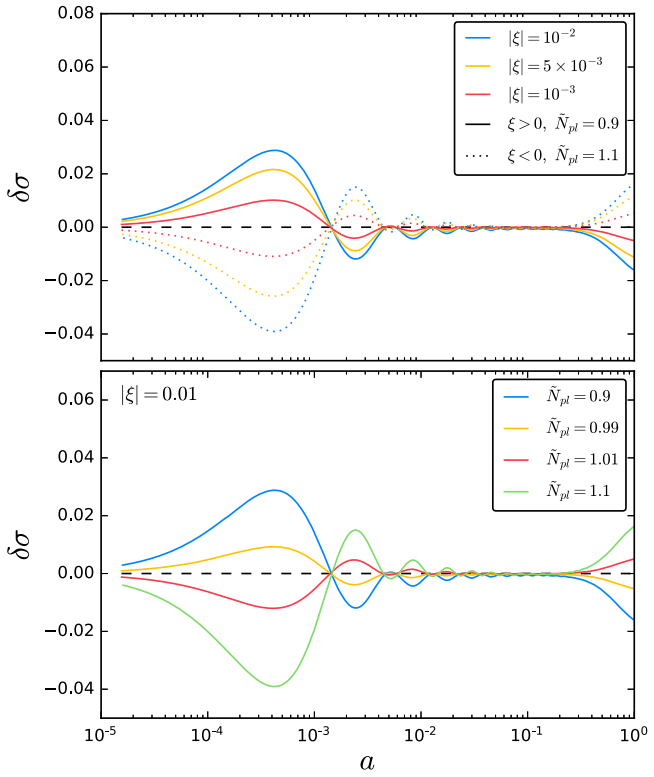

FIG. 10. Evolution of scalar field perturbations in the synchronous gauge for $k = 0.05$ Mpc^{-1}.

As for the homogeneous KG Eq. (10), the choice $V \propto F^2$ also leads to an effectively massless scalar field fluctuation. Both initial conditions for the background and for the linear perturbations at the next-to-leading order in τ are shown in the Appendix. We consider adiabatic initial conditions for the scalar cosmological fluctuations [3,35].

Analogously, the transverse and traceless part of the metric fluctuation h_{ij}^T is expanded as

$$h_{ij}^T = \int \mathrm{d}^3k e^{i\vec{k}\cdot\vec{x}}[h_+ e_{ij}^+ + h_\times e_{ij}^\times], \tag{32}$$

where h_+, h_- and $e^+, e^\times$ are the amplitude and normalized tensors of the two independent states in the direction of propagation of gravitational waves in Fourier space. The evolution equation for the amplitude is

$$\ddot{h}_{s,k} + \left(3H + \frac{\dot{F}}{F}\right)\dot{h}_{s,k} + \frac{k^2}{a^2}h_{s,k} = \frac{2}{F}\rho_\nu\pi^\nu, \tag{33}$$

where s denotes the two polarization states of the two independent modes ($s = +, \times$) and the right-hand side denotes the contribution of the traceless and transverse part of the neutrino anisotropic stress. The importance of the extra damping term in the evolution equation for gravitational waves has previously been stressed [36,37]. The example of the impact of this term with respect

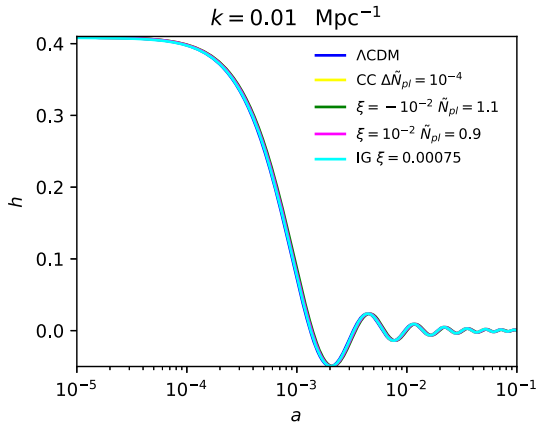

FIG. 11. Evolution of tensor fluctuations h^T for $k = 0.01$ Mpc^{-1}.

to GR is depicted in Fig. 11. Note that the parameters chosen are compatible with the previous figures in this paper, and we are therefore in a regime in which $\dot{F}/F \ll 3H$.

IV. CMB ANISOTROPIES AND MATTER POWER SPECTRA

The footprints of these scalar-tensor theories into the CMB anisotropies angular power spectra can be understood as a generalization of the effects in eJBD or, equivalently,

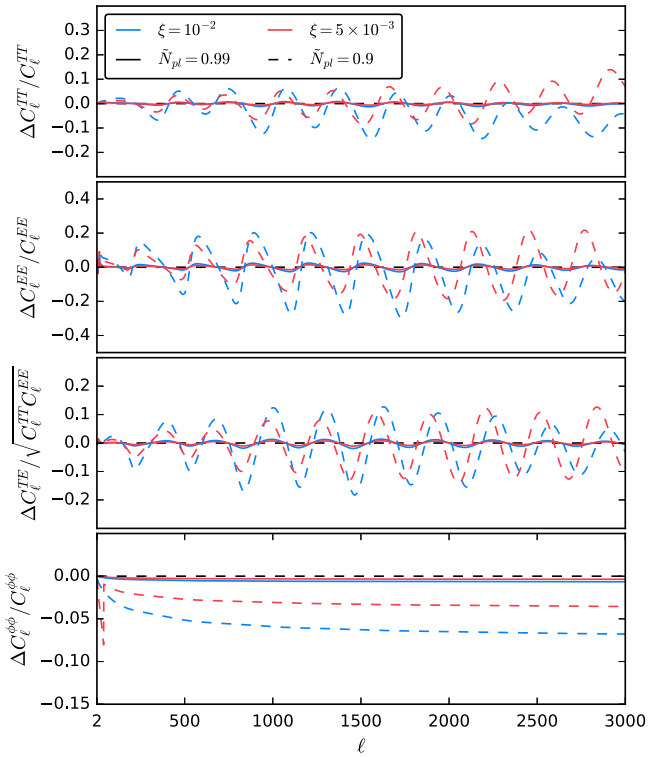

FIG. 12. From top to bottom: Relative differences of the TT-EE-TE-$\phi\phi$ power spectra with respect to the ΛCDM model for $\tilde{N}_{\rm pl} = 1$, 0.9 and different values of $\xi = 10^{-2}, 5 \times 10^{-3}$.

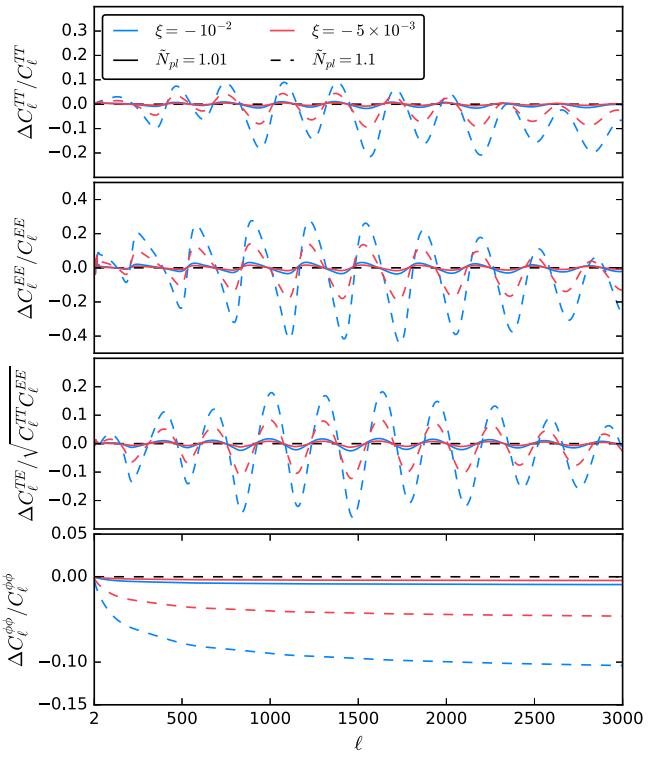

FIG. 13. From top to bottom: Relative differences of the TT-EE-TE-$\phi\phi$ power spectra with respect to the ΛCDM model for $\tilde{N}_{\rm pl} = 1.01$, 1.1 and different values of $\xi = -10^{-2}, -5 \times 10^{-3}$.

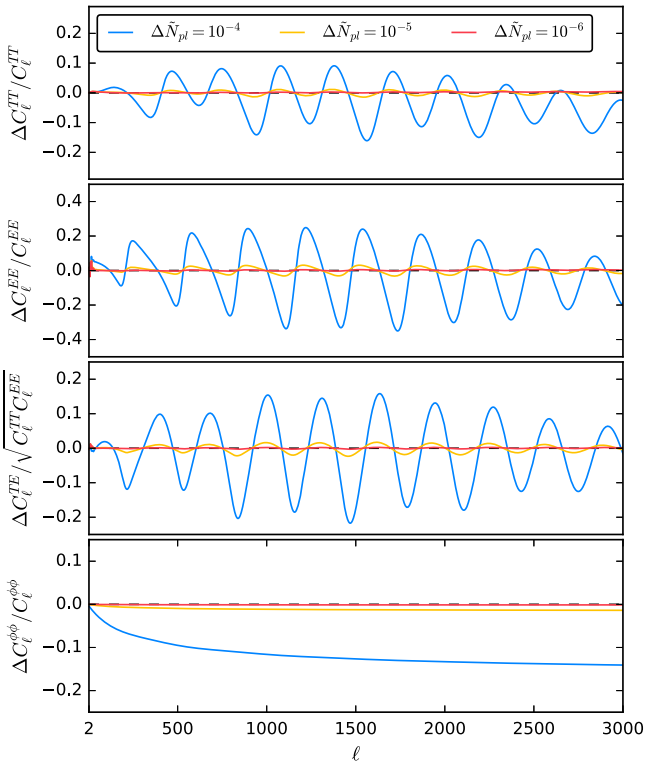

FIG. 14. From top to bottom: Relative differences of the TT-EE-TE-$\phi\phi$ power spectra with respect to the ΛCDM model for the CC case, i.e., $\xi = -1/6$, with different values of $\Delta\tilde{N}_{\rm pl} = 10^{-4}, 10^{-5}, 10^{-6}$.

IG theories. The redshift of matter-radiation equality is modified in scalar-tensor theories by the motion of the scalar field driven by pressureless matter, and this results in a shift of the CMB acoustic peaks for values $\xi \neq 0$, as for the IG case [7,38]. In addition, a departure from $\tilde{N}_{\rm pl} = 1$ induces a further change, both in the amplitude of the peaks and in their positions. We note that decreasing the value of $\tilde{N}_{\rm pl}$ is possible to suppress the deviations with respect to the ΛCDM model, allowing for larger values of the coupling ξ compared to the IG case.

We show the relative differences with respect to the ΛCDM model for the lensed CMB angular power spectra anisotropies in temperature and E-mode polarization, and the CMB lensing angular power spectra for different values of $N_{\rm pl}$ for $\xi > 0$ in Fig. 12, $\xi < 0$ in Fig. 13, and the CC case $\xi = -1/6$ in Fig. 14. We also show the absolute difference of the TE cross-correlation weighted by the square root of the product of the two autocorrelators.

In Fig. 15 we show the relative differences for the matter power spectrum at $z = 0$ with respect to the ΛCDM model for different values of the parameters. In all the cases, the $P(k)$ is enhanced at small scales, i.e., $k \gtrsim 0.01$ h Mpc^{-1}, compared to the ΛCDM model.

We end this section by discussing the B-mode polarization power spectra resulting from the evolution of tensor

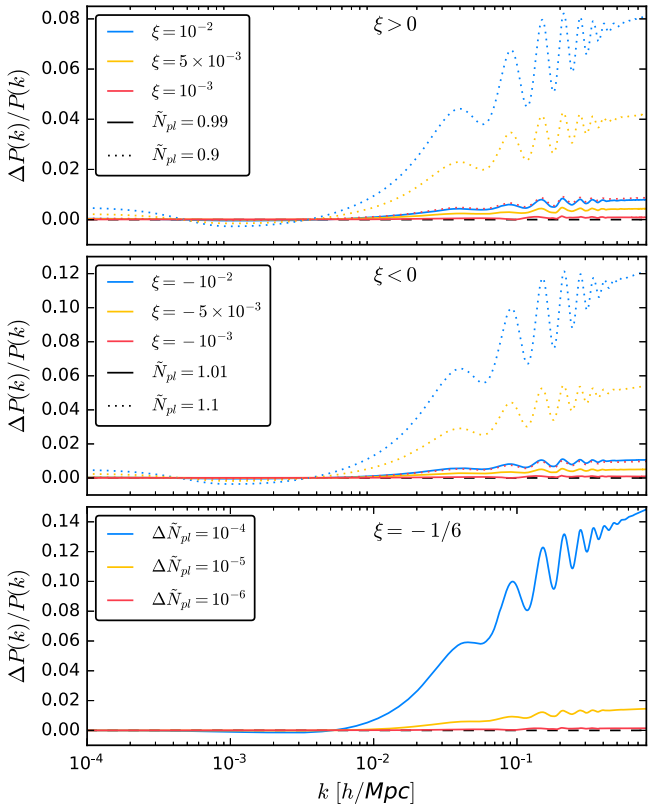

FIG. 15. From top to bottom: Relative differences of the matter power spectra at $z = 0$ with respect to the ΛCDM model for $\xi > 0$, $\xi < 0$, and $\xi = -1/6$.

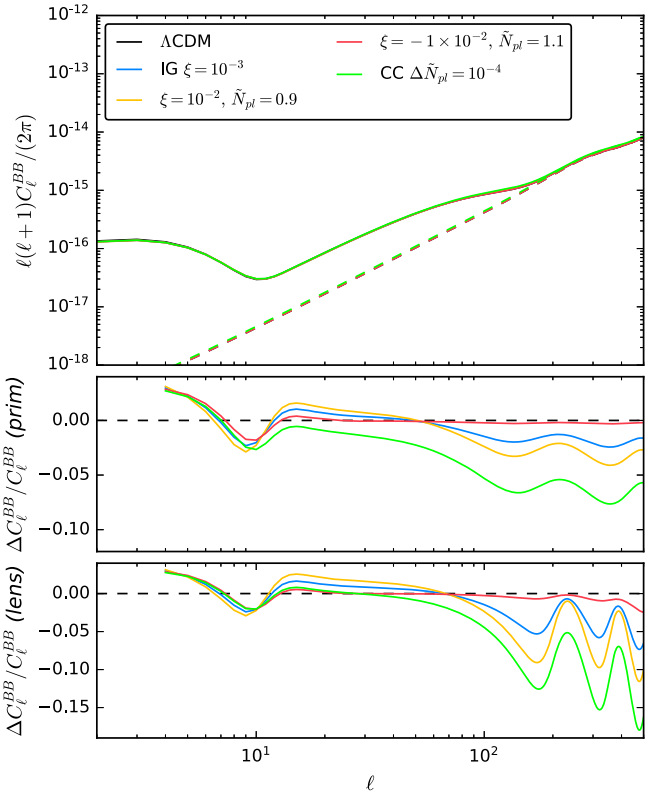

FIG. 16. From top to bottom: CMB B-mode polarization band power, relative differences of the tensor contribution, and relative differences of the lensing contribution with respect to the ΛCDM model for $\xi > 0$, $\xi < 0$, $\xi = -1/6$, and IG. Dashed lines refer to the lensing contribution to the B-mode polarization angular power spectrum.

fluctuations in Eq. (33). Figure 16 shows the comparison of the tensor and lensing contributions to B-mode polarization in ΛCDM GR and the scalar-tensor cases of IG ($N_{\rm pl} = 0$), CC ($\xi = -1/6$), positive and negative ξ for a value of a tensor-to-scalar ratio $r = 0.05$, compatible with the most recent constraints [39,40]. It is important to note that for the values of the couplings chosen in Fig. 16, the main differences in the tensor contribution to B-mode polarization with respect to the ΛCDM GR case is due to the different evolution in the Hubble parameter and in the transfer functions in the definition of CMB anisotropies.

V. CONSTRAINTS FROM COSMOLOGICAL OBSERVATIONS

We perform a Monte Carlo Markov chain analysis by using the publicly available code MontePython[2] [41,42] connected to our modified version of the code `CLASS`[3] [43], i.e., `CLASSig` [3].

[2]See https://github.com/brinckmann/montepython_public.
[3]See https://github.com/lesgourg/class_public.

We use Planck 2015 and BAO likelihoods. We combine the Planck high-ℓ ($\ell > 29$) temperature data with the joint temperature-polarization low-ℓ ($2 \leq \ell \leq 29$) likelihood in pixel space at a resolution of 3.7 deg, i.e., HEALPIX Nside $=$ 16 [44]. The Planck CMB lensing likelihood in the conservative multipoles range, i.e., $40 \leq \ell \leq 400$ [45], from the publicly available Planck 2015 release is also combined. We use BAO data to complement CMB anisotropies at low redshift: We include measurements of D_V/r_s at $z_{\rm eff} = 0.106$ from 6dFGRS [46], at $z_{\rm eff} = 0.15$ from SDSS-MGS [47], and from SDSS-DR11 CMASS and LOWZ at $z_{\rm eff} = 0.57$ and $z_{\rm eff} = 0.32$, respectively [48].

We sample, with linear priors, the six standard cosmological parameters, i.e., $\omega_{\rm b} \equiv \Omega_{\rm b}h^2$, $\omega_{\rm c} \equiv \Omega_{\rm c}h^2$, H_0, $\tau_{\rm re}$, $\ln(10^{10}A_{\rm s})$, and $n_{\rm s}$, plus the two extra parameters for a nonminimally coupled scalar field, i.e., $\Delta\tilde{N}_{\rm pl}$ and ξ. In the analysis we assume massless neutrinos and marginalize over Planck high-ℓ likelihood foreground and calibration nuisance parameters [44] which are allowed to vary.

As in [4], we take into account the change of the cosmological abundances of the light elements during big bang nucleosynthesis (BBN) induced by a different gravitational constant during the radiation era with respect to the theoretical prediction obtained from the public code PArthENoPE [49]. We take into account the modified BBN consistency condition due to the different value of the effective gravitational constant during BBN, by considering this effect as modeled by dark radiation, since the latter effect is already tabulated as $Y_P^{\rm BBN}(\omega_b, N_{\rm eff})$ [50] in the public version of the CLASS code. As in [4], the posterior probabilities for the primary cosmological parameters are hardly affected by the modified BBN consistency condition, and we report a small shift for the primordial helium abundance to higher values.

A. Results

The results from our MCMC exploration are summarized in Table I. We find for the positive branch of the coupling at 95% CL,

$$N_{\rm pl} > 0.81[{\rm M_{pl}}], \tag{34}$$

$$\xi < 0.064. \tag{35}$$

We show in Fig. 17 a zoom of the 2D parameter space (H_0, ξ), comparing the result of NMC scalar fields to IG, i.e., $N_{\rm pl} = 0$. The constraint on ξ is degradated by almost 2 orders of magnitude ($\xi < 0.0075$ at 95% CL for IG [4]) due to the strong degeneracy between $N_{\rm pl}$ and ξ (see Fig. 18).

The constraints for the negative branch are (see Figs. 19 and 20)

$$N_{\rm pl} < 1.39[{\rm M_{pl}}], \tag{36}$$

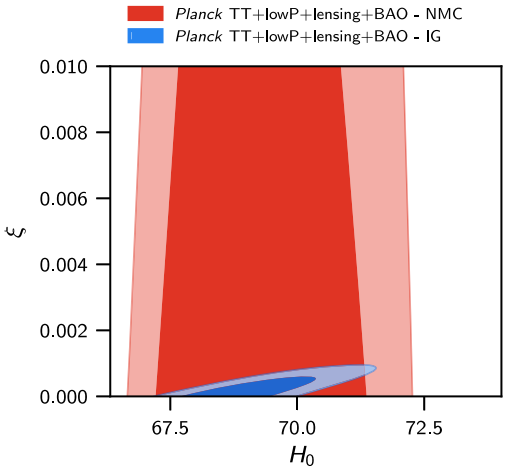

FIG. 17. 2D marginalized confidence levels at 68% and 95% for (H_0, ξ) for NMC $\xi > 0$ (red) and IG (blue) with Planck TT+lowP + lensing + BAO.

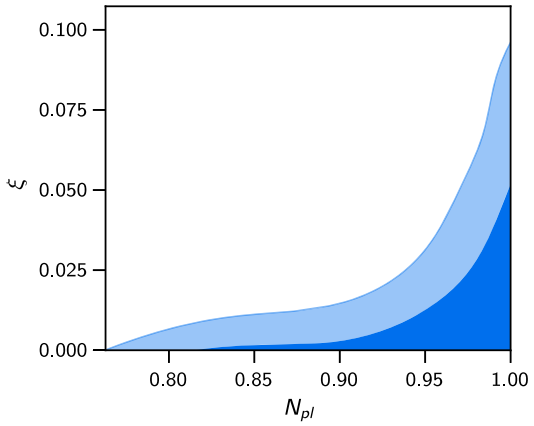

FIG. 18. 2D marginalized confidence levels at 68% and 95% for ($N_{\rm pl}$, ξ) for NMC $\xi > 0$ with Planck TT + lowP + lensing + BAO.

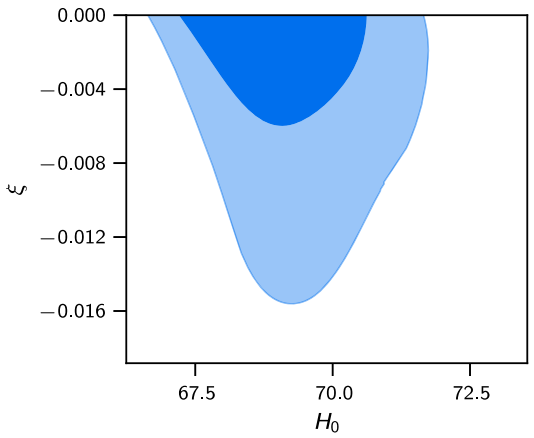

FIG. 19. 2D marginalized confidence levels at 68% and 95% for (H_0, ξ) for NMC $\xi < 0$ with Planck TT + lowP + lensing+ BAO.

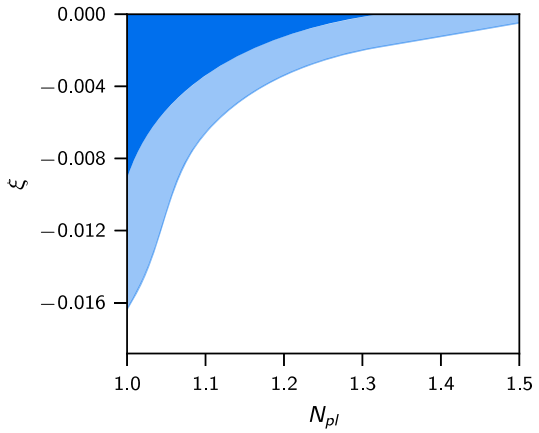

FIG. 20. 2D marginalized confidence levels at 68% and 95% for ($N_{\rm pl}$, ξ) for NMC $\xi < 0$ with Planck TT + lowP + lensing + BAO.

$$\xi > -0.11 \tag{37}$$

at the 95% CL for Planck TT + lowP + lensing + BAO.

We also quote the derived constraints on the change of the effective Newton constant (15) evaluated between the radiation era and the present time, and also its derivative at present time at 95% CL:

$$\frac{\delta G_{\rm eff}}{G} > -0.027, \tag{38}$$

$$\frac{\dot{G}_{\rm eff}}{G}(z=0) > -1.4[\times 10^{-13}\ {\rm yr}^{-1}], \tag{39}$$

for $\xi > 0$, and

$$\frac{\delta G_{\rm eff}}{G} > -0.027, \tag{40}$$

TABLE I. Constraints on the main and derived parameters for Planck TT + lowP + lensing + BAO (at 68% CL if not otherwise stated). In the first column we report the results obtained for the branch with $\xi > 0$, and in the second we give the branch for $\xi < 0$. In the first column we report the results obtained for the ΛCDM model with the same data set [51], and in the second column we give the IG case, i.e., $N_{\rm pl} = 0$, for comparison [4].

	Planck TT+lowP+ lensing+BAO ΛCDM	Planck TT+lowP+ lensing+BAO IG	Planck TT+lowP+ lensing+BAO ($\xi>0$)	Planck TT+lowP+ lensing+BAO ($\xi<0$)
$\omega_{\rm b}$	0.02225 ± 0.00020	$0.02224^{+0.00020}_{-0.00021}$	0.02226 ± 0.00019	0.02226 ± 0.00021
$\omega_{\rm c}$	0.1186 ± 0.0012	0.1191 ± -0.0014	0.1190 ± 0.0015	0.1189 ± 0.0015
H_0 [kms^{-1}Mpc^{-1}]	67.78 ± 0.57	$69.4^{+0.7}_{-0.9}$	$69.2^{+0.8}_{-1.1}$	$69.2^{+0.7}_{-1.0}$
$\tau_{\rm re}$	0.066 ± 0.012	$0.063^{+0.012}_{-0.014}$	0.068 ± 0.014	0.069 ± 0.013
$\ln(10^{10}A_{\rm s})$	3.062 ± 0.024	$3.059^{+0.022}_{-0.026}$	$3.069^{+0.023}_{-0.027}$	3.071 ± 0.024
$n_{\rm s}$	0.9675 ± 0.0045	$0.9669^{+0.0042}_{-0.0047}$	0.9674 ± 0.0046	0.9728 ± 0.0043
ξ	…	<0.00075 (95% CL)	<0.064 (95% CL)	>-0.011 (95% CL)
$N_{\rm pl}$ [$M_{\rm pl}$]	…	0	>0.81 (95% CL)	<1.39 (95% CL)
$\gamma_{\rm PN}$	1	>0.9970 (95% CL)	>0.995 (95% CL)	>0.997 (95% CL)
$\beta_{\rm PN}$	1	1	>0.99987 (95% CL)	<1.000011 (95% CL)
$\delta G_{\rm N}/G_{\rm N}$	…	$-0.009^{+0.003}_{-0.009}$	>-0.027 (95% CL)	>-0.027 (95% CL)
$10^{13}\dot{G}_{\rm N}(z=0)/G_{\rm N}$ [yr^{-1}]	…	-0.37^{+34}_{-12}	>-1.4 (95% CL)	>-0.97 (95% CL)

TABLE II. Constraints on main and derived parameters for Planck TT + lowP + lensing + BAO in the case of the CC model (at 68% CL if not otherwise stated).

	Planck TT + lowP + lensing + BAO	Planck TT + lowP + lensing + BAO + HST
$\omega_{\rm b}$	0.02223 ± 0.00021	0.02228 ± 0.00021
$\omega_{\rm c}$	$0.1188^{+0.0014}_{-0.0015}$	0.1187 ± 0.0015
H_0 [km s^{-1} Mpc^{-1}]	$69.19^{+0.77}_{-0.93}$	70.20 ± 0.83
$\tau_{\rm re}$	$0.068^{+0.012}_{-0.014}$	$0.070^{+0.013}_{-0.015}$
$\ln(10^{10}A_{\rm s})$	3.070 ± 0.024	3.074 ± 0.024
$n_{\rm s}$	0.9699 ± 0.0045	0.9728 ± 0.0043
$N_{\rm pl}$ [$M_{\rm pl}$]	< 1.000038 (95% CL)	$1.000028^{+0.000012}_{-0.000014}$
$\gamma_{\rm PN}$	> 0.99996 (95% CL)	0.99997 ± 0.00001
$\beta_{\rm PN}$	< 1.000003 (95% CL)	1.000002 ± 0.000001

$$\frac{\dot{G}_{\rm eff}}{G}(z=0) > -0.97[\times 10^{-13}\ {\rm yr}^{-1}], \tag{41}$$

for $\xi < 0$.

For the CC case, i.e., fixing $\xi = -1/6$, results are listed in Table II. This model is severely constrained by data, leading to a tight upper bound on $N_{\rm pl}$ at 95% CL:

$$1 < N_{\rm pl} < 1.000038[{\rm M_{pl}}], \tag{42}$$

where $\tilde{N}_{\rm pl}$ can take only values larger than 1 in this case.

All these models provide a fit to Planck 2015 and BAO data very similar to ΛCDM: We report $\Delta\chi^2 \sim -2.6$ for all the models considered in this paper. Because of the limited improvement in $\Delta\chi^2$, none of these models is preferred at a statistically significant level with respect to ΛCDM.

B. The Hubble parameter

We find constraints compatible with the ΛCDM values for the standard cosmological parameters. However, the shifts in H_0 deserve a particular mention: As already remarked in [3,4] for the IG case, the mean values for H_0 are larger for all the models studied here. Figure 21 shows how the 2D marginalized contours for (H_0, $N_{\rm pl}$) have a degeneracy. We find

$$H_0 = 69.19^{+0.77}_{-0.93}\ [{\rm km/s/Mpc}]. \tag{43}$$

This value is larger but compatible at the 2σ level with the ΛCDM value ($H_0 = 67.78 \pm 0.57$ [km/s/Mpc]). However, it is still lower than the local measurement of the Hubble constant [52] ($H_0 = 73.52 \pm 1.62$ [km/s/Mpc]) obtained by including the new MW parallaxes from HST and Gaia in the rest of the data from [53]. Therefore, the tension between the model dependent estimate of the Hubble parameter from Planck 2015 plus BAO data and the local measurement from [52] decreases to 2.3σ from the 3.3σ of the ΛCDM model. For comparison, by varying the number of degrees of relativistic species, $N_{\rm eff}$, in Einstein gravity, a lower value for the Hubble parameter, i.e., $H_0 = 68.00 \pm 1.5$ [km/s/Mpc] (with $N_{\rm eff} = 3.08^{+0.22}_{-0.24}$) for Planck TT + lowP + lensing + BAO at 68% CL, is obtained compared to the CC case reported in Eq. (43). When the local measurement of the Hubble constant [52] is included in the fit, we obtain

$$H_0 = 70.20 \pm 0.83\ [{\rm km/s/Mpc}], \tag{44}$$

$$N_{\rm pl} = 1.000028^{+0.000012}_{-0.000014}\ [{\rm M_{pl}}]. \tag{45}$$

Since the marginalized value for H_0 in either eJBD or NMC models is larger than in common extensions of the ΛCDM model [51], such as ΛCDM + $N_{\rm eff}$, it is useful to understand how the evolution of the Hubble parameter differs at early and late times. The differences at early time can be easily understood: Since the effective Newton constant can only decrease, if we consider the same H_0, this will correspond to a higher $H(z)$ or to a larger $N_{\rm eff}$ in

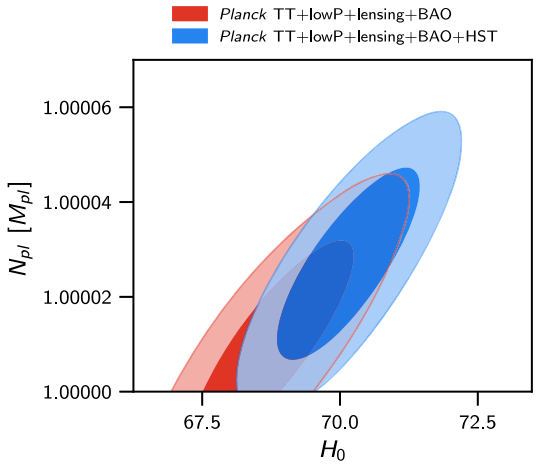

FIG. 21. 2D marginalized confidence levels at 68% and 95% for (H_0, $N_{\rm pl}$) for conformal coupling with Planck TT + lowP + lensing + BAO. We include in blue the local estimates of $H_0 = 73.52 \pm 1.62$ [km/s/Mpc] [52].

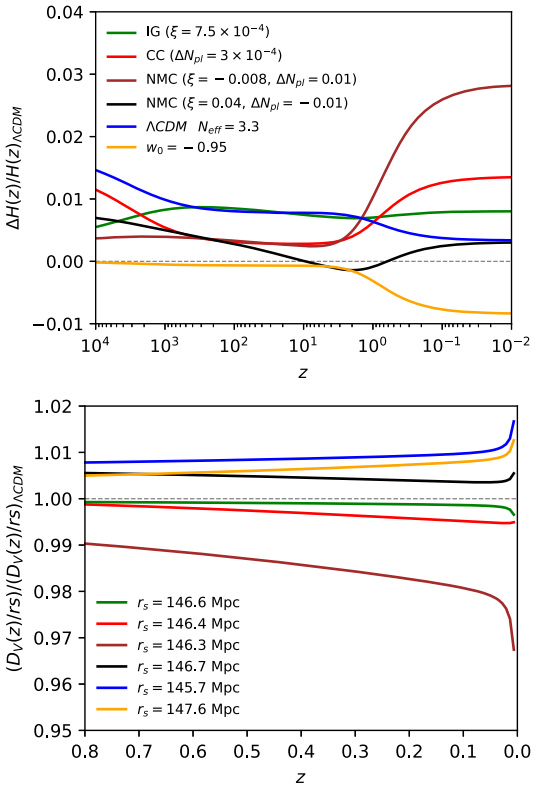

FIG. 22. Redshift evolution for the relative difference between the Hubble parameter $H(z)$ and its ΛCDM counterpart (upper panel) and the ratio $D_V(z)/r_s$ (lower panel). For ΛCDM quantities we use Planck TT + lowP + lensing + BAO best fit. The models plotted are IG, CC, $\xi < 0$, $\xi > 0$, the ΛCDM model with $N_{\rm eff} > 3.046$, and the wCDM with $w_0 = {\rm const} \neq 0$ for green, red, brown, black, blue, and orange lines, respectively.

the radiation era compared to the ΛCDM. A second effect around recombination is the motion of the scalar field driven by pressureless matter. At lower redshifts, the differences with respect to ΛCDM are originated by the onset of the acceleration stage by σ. The upper panel of Fig. 22 shows relative differences of $H(z)$ with respect to the Planck TT + lowP + lensing + BAO ΛCDM best fit: Best-fit (for IG) or NMC models within the 1σ contours are compared with ΛCDM + $N_{\rm eff}$ or wCDM. This plot shows how, in these scalar-tensor models, both early and late time dynamics can contribute to a larger value for H_0 than in ΛCDM + $N_{\rm eff}$, for example.

However, because of this contribution from late time dynamics, the change in H_0 cannot be interpreted only as a proportional decrement in the comoving sound horizon at the baryon drag epoch r_s, which is the quantity used to calibrate the BAO standard ruler and is 147.6 Mpc for ΛCDM with the data considered. The bottom panel of Fig. 22 shows $D_V(z)/r_s \equiv \frac{[cz(1+z)^2 D_A(z)^2 H(z)^{-1}]^{1/3}}{r_s}$, with D_A the angular diameter distance, normalized to its ΛCDM value, and the value of r_s. It is easy to see that both r_s and H_0 are lower for ΛCDM + $N_{\rm eff}$ than for the scalar-tensor models studied here and the eJBD model. These scalar-tensor models therefore differ from those which aim in reducing the tension between CMB anisotropies and the local measurements of H_0 through a decrement of r_s [54–56], such as those in which ultralight axion fields move slowly around recombination and then dilute away [57–59]. In the scalar-tensor models considered here, the scalar field moves naturally around recombination since it is forced by pressureless matter and dominates at late time acting as DE.

C. Constraints on the post-Newtonian parameters

Finally, we quote the derived constraints on the post-Newtonian parameters. In this class of models $\gamma_{\rm PN}, \beta_{\rm PN} \neq 1$ according to Eqs. (22) and (23) at 95% CL:

$$0.995 < \gamma_{\rm PN} < 1 \ (\xi > 0), \tag{46}$$

$$0.99987 < \beta_{\rm PN} < 1, \tag{47}$$

$$0.997 < \gamma_{\rm PN} < 1 \ (\xi < 0), \tag{48}$$

$$1 < \beta_{\rm PN} < 1.000011. \tag{49}$$

See Fig. 23 for the 2D marginalized constraints in the $(\gamma_{\rm PN}, \beta_{\rm PN})$ plane. See Fig. 24 for the 2D marginalized constraints in the $(H_0, \gamma_{\rm PN})$ plane for $\xi > 0$ compared to the IG case studied in [4].

The tight constraint on $N_{\rm pl}$ for the CC case corresponds at 95% CL to

$$0 < 1 - \gamma_{\rm PN} < 4 \times 10^{-5}, \tag{50}$$

$$0 < \beta_{\rm PN} - 1 < 3 \times 10^{-6}, \tag{51}$$

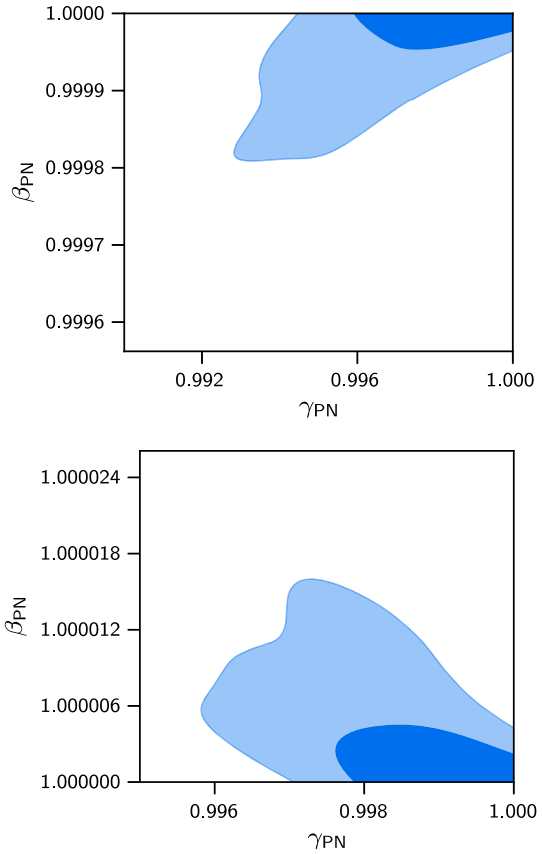

FIG. 23. 2D marginalized confidence levels at 68% and 95% for $(\gamma_{\rm PN}, \beta_{\rm PN})$ for NMC $\xi > 0$ (left panel) and $\xi < 0$ (right panel) with Planck TT + lowP + lensing + BAO.

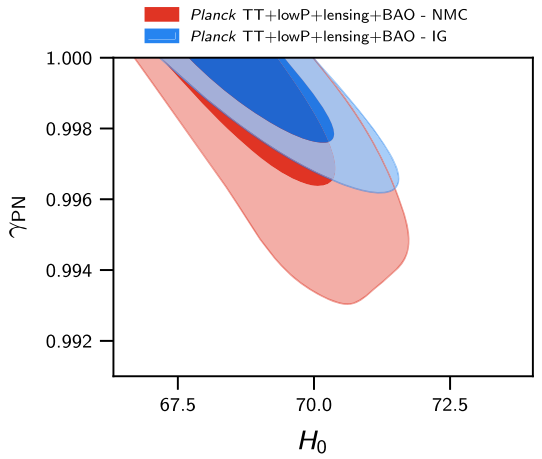

FIG. 24. 2D marginalized confidence levels at 68% and 95% for $(H_0, \gamma_{\rm PN})$ for NMC $\xi > 0$ (red) and IG (blue) with Planck TT + lowP + lensing + BAO.

for Planck TT + lowP + lensing + BAO, where the latter is tighter than the constraint from the perihelion shift $\beta_{\rm PN} - 1 = (4.1 \pm 7.8) \times 10^{-5}$ [60] and the former is twice the uncertainty of the Shapiro time delay constraint $\gamma_{\rm PN} - 1 = (2.1 \pm 2.3) \times 10^{-5}$ [61].

VI. CONCLUSIONS

We have expanded on our previous study of the observational predictions within the eJBD theory or, equivalently, IG [3,4], to the case of a scalar field nonminimally coupled to the Einstein gravity as in Eq. (1) with $G_3 = G_5 = 0$ and $2G_4 = F(\sigma) = N_{\rm pl}^2 + \xi\sigma^2$. We have studied this class of models under the assumption that the effective gravitational constant in these scalar-tensor theories is compatible with the one measured in a Cavendish-like experiment. Whereas in the eJBD theory only the first post-Newtonian parameter $\gamma_{\rm PN}$ $(= 1 - \frac{F_{,\sigma}^2}{F+2F_{,\sigma}^2})$ is nonvanishing, in this simple extension both the first and second post-Newtonian parameters $\beta_{\rm PN}$ $(= 1 + \frac{FF_{,\sigma}}{8F+12F_{,\sigma}^2}\frac{d\gamma_{\rm PN}}{d\sigma})$ are nonzero. The second post-Newtonian parameter encodes the sign of the coupling to gravity, i.e., $\beta_{\rm PN} > 0$ (< 0) for $\xi > 0$ $(\xi < 0)$.

For the sake of simplicity, we have restricted ourselves to the class of potential $V(\sigma) \propto F^2(\sigma)$, which makes the field effectively massless [19] and allows for a direct comparison with the IG model for $N_{\rm pl} = 0$ [3,4,28,33,62]. For this choice of potential $V(\sigma) \propto F^2(\sigma)$, the scalar field is effectively massless. By assuming natural initial conditions in which the decaying mode is negligible, the scalar field starts at rest deep in the radiation era and is pushed by pressureless matter to the final stage in which it drives the Universe in a nearly de Sitter stage at late times with $\sigma = $ const. In general, the effective parameter of state $w_{\rm DE}$ for σ defined in [31] tracks the one of the dominant matter component before reaching -1 once the Universe enters the accelerated stage as for the IG case. We find that the conformal case $\xi = -1/6$ is an exception to this general trend: For such a value the effective parameter of state $w_{\rm DE}$ interpolates between $1/3$ and -1 without an intermediate pressureless stage. Irrespective of the sign of the coupling ξ, $G_N(a) = 1/(8\pi F)$ decrease with time for this class of potentials.

As in our previous works in IG, we have considered adiabatic initial conditions for fluctuations [3,4,63] which are derived in this work for a nonminimally coupled scalar field. By extending the modification of `CLASSig` [3] to a generic coupling $F(\sigma)$, we have derived the CMB temperature and polarization anisotropies and the matter power spectrum. Since the effective Newton constant decreases in time after the relativistic era, we observe a shift of the acoustic peaks to higher multipoles and an excess in the matter power spectrum at $k \gtrsim 0.01$ Mpc^{-1} proportional to the deviation from GR.

We have used Planck 2015 and BAO data to constrain this class of models. As for IG, we obtain a marginalized value for H_0 higher than in ΛCDM for all these models, potentially alleviating the tension with the local measurement of the Hubble parameter obtained by calibrating with the Cepheids [52]. The goodness of fit to Planck 2015 plus BAO data provided by the models studied in this paper is quantitatively similar to ΛCDM: Since they have one (for the conformal coupled case $\xi = -1/6$) or two (for ξ allowed to vary) extra parameters, these models are not preferred with respect to ΛCDM. We have derived 95% CL upper bounds $\xi < 0.064$ $(|\xi| < 0.11)$ and $0.81 < N_{\rm pl} < 1$ $(1 < N_{\rm pl} < 1.39)$ for $\xi > 0$ $(\xi < 0)$. It is interesting to note that the bounds on $\gamma_{\rm PN}$ and $\delta G_{\rm eff}/G$ have just a small degradation with respect to eJBD with the same data set $(0.997 < \gamma_{\rm PN} < 1$ [4]). Overall, some cosmological constraints do not seem strongly dependent on the assumption $\beta_{\rm PN} = 0$, and they have a large margin of improvement with future observations [14]. Although model dependent, cosmological observations seem more promising than other independent ways to test scalar-tensor theories in the strong gravity regime as the search for the presence of scalar polarization states of gravita- tional waves [64], which is also strongly constrained by LIGO/Virgo [65].

The conformal value $\xi = -1/6$ is an interesting and particular case which stands out within the general class of nonminimally coupled scalar fields. In addition to what was already remarked about its effective parameter of state, we find that Planck 2015 + BAO data quite tightly constrain the conformal case with $V(\sigma) \propto F^2(\sigma)$: As 95% CL intervals, we find $1 < 10^5\Delta\tilde{N}_{\rm Pl} < 3.8$, or equivalently $0.99996 < \gamma_{\rm PN} < 1$, $1 < \beta_{\rm PN} < 1.000003$, in terms of the post-Newtonian parameters. These tight cosmological constraints for the conformal case are comparable to those obtained within the Solar System bounds [61].

From Figs. 12–16, we see that CMB polarization anisotropies have a greater sensitivity to the variation of the gravitational strength in these models. It will therefore be interesting to see the impact of the latest and more robust measurement of CMB polarization anisotropies from Planck [66–68] and from the BICEP2/Keck Array [66] as well as of the more recent BAO data on the constraints of these models.

ACKNOWLEDGMENTS

We would like to thank Lloyd Knox and Vivian Poulin for discussions. M. Ba. was supported by the South African Radio Astronomy Observatory, which is a facility of the National Research Foundation, an agency of the Department of Science and Technology, and he was also supported by the Claude Leon Foundation. M. Ba., M. Br., F. F., and D. P. acknowledge financial contributions from ASI/INAF Agreement No. 2018-23-HH.0 "Attività scientifica per la missione EUCLID—Fase D." F. F. and D. P. also acknowledge financial support from ASI Grant No. 2016-24-H.0. A. A. S. was partly supported by the program KP19-270 "Questions of the origin and evolution of the Universe" of the Presidium of the Russian Academy of Sciences. This research used computational resources of the National Energy Research Scientific Computing Center (NERSC) and of INAF OAS Bologna.

APPENDIX: INITIAL CONDITIONS

Here we report the initial conditions adopted in this paper for a nonminimally coupled scalar field, which generalize the case of adiabatic initial conditions for IG presented in [63]. These quantities reduce to IG and general relativity cases for $N_{\rm pl} = 0$ and ($N_{\rm pl} = M_{\rm pl}$, $\xi = 0$), respectively.

For the background cosmology we have as initial conditions

$$a(\tau) = \sqrt{\frac{\rho_{r0}}{3F_i}}\tau\left[1 + \frac{\omega}{4}\tau - \frac{5}{16}\frac{\xi^2\sigma_i^2(1+6\xi)}{F_i + 6\xi^2\sigma_i^2}\omega^2\tau^2\right], \tag{A1}$$

$$\mathcal{H}(\tau) = \frac{1}{\tau}\left[1 + \frac{\omega}{4}\tau - \frac{1}{16}\frac{F_i + 4\xi^2\sigma_i^2(4+15\xi)}{F_i + 6\xi^2\sigma_i^2}\omega^2\tau^2\right], \tag{A2}$$

$$\sigma(\tau) = \sigma_i\left[1 + \frac{3}{2}\xi\omega\tau - \frac{2F_i(1-3\xi) + 27\xi^2\sigma_i^2(1+2\xi)}{8(F_i + 6\xi^2\sigma_i^2)}\omega^2\tau^2\right], \tag{A3}$$

where $\omega = \frac{\rho_{m0}}{\sqrt{3\rho_{r0}}}\frac{\sqrt{F_i}}{F_i + 6\xi^2\sigma_i^2}$.

For cosmological fluctuations in the synchronous gauge, we have as adiabatic initial conditions

$$\delta_\gamma(k,\tau) = \delta_\nu(k,\tau) = \frac{4}{3}\delta_b(k,\tau) = \frac{4}{3}\delta_c(k,\tau) = -\frac{1}{3}k^2\tau^2\left(1 - \frac{\omega}{5}\tau\right), \tag{A4}$$

$$\theta_c(k,\tau) = 0, \tag{A5}$$

$$\theta_\gamma(k,\tau) = \theta_b(k,\tau) = -\frac{k^4\tau^3}{36}\left[1 - \frac{3}{20}\frac{F_i(1 - R_\nu + 5R_b) + 30\xi^2\sigma_i^2}{(1-R_\nu)F_i}\omega\tau\right], \tag{A6}$$

$$\theta_\nu(k,\tau) = -\frac{k^4\tau^3}{36}\left[\frac{23 + 4R_\nu}{15 + 4R_\nu} - \frac{3(275 + 50R_\nu + 8R_\nu^2)F_i - 180(-5 + 4R_\nu)\xi^2\sigma_i^2}{20(15 + 2R_\nu)(15 + 4R_\nu)F_i}\omega\tau\right], \tag{A7}$$

$$\sigma_\nu(k,\tau) = \frac{2k^2\tau^2}{3(15 + 4R_\nu)}\left[1 + \frac{(-5 + 4R_\nu)(F + 6\xi^2\sigma_i^2)}{4(15 + 2R_\nu)F_i}\omega\tau\right], \tag{A8}$$

$$\eta(k,\tau) = 1 - \frac{k^2\tau^2}{12}\left[\frac{5 + 4R_\nu}{15 + 4R_\nu} - \frac{150(-5 + 4R_\nu)\xi^2\sigma_i^2 + (325 + 280R_\nu + 16R_\nu^2)F_i}{10(15 + 4R_\nu)(15 + 2R_\nu)F_i}\omega\tau\right], \tag{A9}$$

$$h(k,\tau) = \frac{k^2\tau^2}{2}\left(1 - \frac{\omega}{5}\tau\right), \tag{A10}$$

$$\delta\sigma(k,\tau) = -\frac{1}{8}k^2\tau^3\xi\omega\sigma_i\left[1 - \frac{2\xi^2\sigma_i^2(24 + 45\xi) + (4 - 9\xi)F_i}{10(F_i + 6\xi^2\sigma_i^2)}\omega\tau\right], \tag{A11}$$

where $R_\nu = \frac{\rho_{\nu 0}}{\rho_{r0}}$ and $R_b = \frac{\rho_{b0}}{\rho_{m0}}$.

[1] J.-P. Uzan, Varying constants, gravitation and cosmology, Living Rev. Relativity **14**, 2 (2011).

[2] P. A. R. Ade *et al.* (Planck Collaboration), Planck 2013 results. XVI. Cosmological parameters, Astron. Astrophys. **571**, A16 (2014).

[3] C. Umiltà, M. Ballardini, F. Finelli, and D. Paoletti, CMB and BAO constraints for an induced gravity dark energy model with a quartic potential, J. Cosmol. Astropart. Phys. 08 (2015) 017.

[4] M. Ballardini, F. Finelli, C. Umiltà, and D. Paoletti, Cosmological constraints on induced gravity dark energy models, J. Cosmol. Astropart. Phys. 05 (2016) 067.

[5] P. Jordan, Formation of the stars and development of the Universe, Nature (London) **164**, 637 (1949).

[6] C. Brans and R. H. Dicke, Mach's principle and a relativistic theory of gravitation, Phys. Rev. **124**, 925 (1961).

[7] X.-l. Chen and M. Kamionkowski, Cosmic microwave background temperature and polarization anisotropy in Brans-Dicke cosmology, Phys. Rev. D **60**, 104036 (1999).

[8] R. Nagata, T. Chiba, and N. Sugiyama, WMAP constraints on scalar-tensor cosmology and the variation of the gravitational constant, Phys. Rev. D **69**, 083512 (2004).

[9] V. Acquaviva, C. Baccigalupi, S. M. Leach, A. R. Liddle, and F. Perrotta, Structure formation constraints on the Jordan-Brans-Dicke theory, Phys. Rev. D **71**, 104025 (2005).

[10] A. Avilez and C. Skordis, Cosmological Constraints on Brans-Dicke Theory, Phys. Rev. Lett. **113**, 011101 (2014).

[11] Y.-C. Li, F.-Q. Wu, and X. Chen, Constraints on the Brans-Dicke gravity theory with the Planck data, Phys. Rev. D **88**, 084053 (2013).

[12] J. Ooba, K. Ichiki, T. Chiba, and N. Sugiyama, Planck constraints on scalar-tensor cosmology and the variation of the gravitational constant, Phys. Rev. D **93**, 122002 (2016).

[13] G. Walter Horndeski, Second-order scalar-tensor field equations in a four-dimensional space, Int. J. Theor. Phys. **10**, 363 (1974).

[14] M. Ballardini, D. Sapone, C. Umiltà, F. Finelli, and D. Paoletti, Testing extended Jordan-Brans-Dicke theories with future cosmological observations, J. Cosmol. Astropart. Phys. 05 (2019) 049.

[15] D. Alonso, E. Bellini, P. G. Ferreira, and M. Zumalacárregui, Observational future of cosmological scalar-tensor theories, Phys. Rev. D **95**, 063502 (2017).

[16] J.-P. Uzan, Cosmological scaling solutions of nonminimally coupled scalar fields, Phys. Rev. D **59**, 123510 (1999).

[17] F. Perrotta, C. Baccigalupi, and S. Matarrese, Extended quintessence, Phys. Rev. D **61**, 023507 (1999).

[18] N. Bartolo and M. Pietroni, Scalar tensor gravity and quintessence, Phys. Rev. D **61**, 023518 (1999).

[19] L. Amendola, Scaling solutions in general nonminimal coupling theories, Phys. Rev. D **60**, 043501 (1999).

[20] T. Chiba, Quintessence, the gravitational constant, and gravity, Phys. Rev. D **60**, 083508 (1999).

[21] T. Baker, E. Bellini, P. G. Ferreira, M. Lagos, J. Noller, and I. Sawicki, Strong Constraints on Cosmological Gravity from GW170817 and GRB 170817A, Phys. Rev. Lett. **119**, 251301 (2017).

[22] P. Creminelli and F. Vernizzi, Dark Energy after GW170817 and GRB170817A, Phys. Rev. Lett. **119**, 251302 (2017).

[23] J. María Ezquiaga and M. Zumalacárregui, Dark Energy after GW170817: Dead Ends and the Road Ahead, Phys. Rev. Lett. **119**, 251304 (2017).

[24] B. P. Abbott *et al.* (LIGO scientific and Virgo Collaboration), GW170817: Observation of Gravitational Waves from a Binary Neutron Star Inspiral, Phys. Rev. Lett. **119**, 161101 (2017).

[25] L. Lombriser and A. Taylor, Breaking a dark degeneracy with gravitational waves, J. Cosmol. Astropart. Phys. 03 (2016) 031.

[26] L. Lombriser and N. A. Lima, Challenges to self-acceleration in modified gravity from gravitational waves and large-scale structure, Phys. Lett. B **765**, 382 (2017).

[27] C. Wetterich, Cosmology and the fate of dilatation symmetry, Nucl. Phys. **B302**, 668 (1988).

[28] F. Cooper and G. Venturi, Cosmology and broken scale invariance, Phys. Rev. D **24**, 3338 (1981).

[29] A. Cerioni, F. Finelli, A. Tronconi, and G. Venturi, Inflation and reheating in induced gravity, Phys. Lett. B **681**, 383 (2009).

[30] F. L. Bezrukov and M. Shaposhnikov, The Standard Model Higgs boson as the inflaton, Phys. Lett. B **659**, 703 (2008).

[31] B. Boisseau, G. Esposito-Farese, D. Polarski, and Alexei A. Starobinsky, Reconstruction of a Scalar Tensor Theory of Gravity in an Accelerating Universe, Phys. Rev. Lett. **85**, 2236 (2000).

[32] R. Gannouji, D. Polarski, A. Ranquet, and A. A. Starobinsky, Scalar-tensor models of normal and phantom dark energy, J. Cosmol. Astropart. Phys. 09 (2006) 016.

[33] F. Finelli, A. Tronconi, and Giovanni Venturi, Dark energy, induced gravity and broken scale invariance, Phys. Lett. B **659**, 466 (2008).

[34] C.-P. Ma and E. Bertschinger, Cosmological perturbation theory in the synchronous and conformal Newtonian gauges, Astrophys. J. **455**, 7 (1995).

[35] M. Rossi, Dark energy as a scalar field non-minimally coupled to gravity (2016).

[36] A. Riazuelo and J.-P. Uzan, Quintessence and gravitational waves, Phys. Rev. D **62**, 083506 (2000).

[37] L. Amendola, G. Ballesteros, and V. Pettorino, Effects of modified gravity on B-mode polarization, Phys. Rev. D **90**, 043009 (2014).

[38] A. R. Liddle, A. Mazumdar, and J. D. Barrow, Radiation matter transition in Jordan-Brans-Dicke theory, Phys. Rev. D **58**, 027302 (1998).

[39] Y. Akrami *et al.* (Planck Collaboration), Planck 2018 results. X. Constraints on inflation, arXiv:1807.06211.

[40] P. A. R. Ade *et al.* (BICEP2 and Keck Array Collaboration), BICEP2/Keck Array x: Constraints on Primordial Gravitational Waves using Planck, WMAP, and New BICEP2/Keck Observations through the 2015 Season, Phys. Rev. Lett. **121**, 221301 (2018).

[41] B. Audren, J. Lesgourgues, K. Benabed, and S. Prunet, Conservative constraints on early cosmology: An illustration of the Monte Python cosmological parameter inference code, J. Cosmol. Astropart. Phys. 02 (2013) 001.

[42] T. Brinckmann and J. Lesgourgues, MontePython 3: Boosted MCMC sampler and other features, arXiv:1804.07261.

[43] D. Blas, J. Lesgourgues, and T. Tram, The cosmic linear anisotropy solving system (CLASS) II: Approximation schemes, J. Cosmol. Astropart. Phys. 07 (2011) 034.
[44] N. Aghanim *et al.* (Planck Collaboration), Planck 2015 results. XI. CMB power spectra, likelihoods, and robustness of parameters, Astron. Astrophys. **594**, A11 (2016).
[45] P. A. R. Ade *et al.* (Planck Collaboration), Planck 2015 results. XV. Gravitational lensing, Astron. Astrophys. **594**, A15 (2016).
[46] F. Beutler, C. Blake, M. Colless, D. Heath Jones, L. Staveley-Smith, L. Campbell, Q. Parker, W. Saunders, and F. Watson, The 6dF Galaxy survey: Baryon acoustic oscillations and the local hubble constant, Mon. Not. R. Astron. Soc. **416**, 3017 (2011).
[47] L. Anderson *et al.* (BOSS Collaboration), The clustering of galaxies in the SDSS-III Baryon oscillation spectroscopic Survey: Baryon acoustic oscillations in the data releases 10 and 11 Galaxy samples, Mon. Not. R. Astron. Soc. **441**, 24 (2014).
[48] A. J. Ross, L. Samushia, C. Howlett, W. J. Percival, A. Burden, and M. Manera, The clustering of the SDSS DR7 main Galaxy sample—I. A 4 per cent distance measure at $z = 0.15$, Mon. Not. R. Astron. Soc. **449**, 835 (2015).
[49] O. Pisanti, A. Cirillo, S. Esposito, F. Iocco, G. Mangano, G. Miele, and P. D. Serpico, PArthENoPE: Public algorithm evaluating the nucleosynthesis of primordial elements, Comput. Phys. Commun. **178**, 956 (2008).
[50] J. Hamann, J. Lesgourgues, and G. Mangano, Using BBN in cosmological parameter extraction from CMB: A forecast for PLANCK, J. Cosmol. Astropart. Phys. 03 (2008) 004.
[51] P. A. R. Ade *et al.* (Planck Collaboration), Planck 2015 results. XIII. Cosmological parameters, Astron. Astrophys. **594**, A13 (2016).
[52] A. G. Riess *et al.*, Milky Way cepheid standards for measuring cosmic distances and application to Gaia DR2: Implications for the Hubble constant, Astrophys. J. **861**, 126 (2018).
[53] A. G. Riess *et al.*, A 2.4% determination of the local value of the Hubble constant, Astrophys. J. **826**, 56 (2016).
[54] A. J. Cuesta, L. Verde, A. Riess, and R. Jimenez, Calibrating the cosmic distance scale ladder: The role of the sound horizon scale and the local expansion rate as distance anchors, Mon. Not. R. Astron. Soc. **448**, 3463 (2015).
[55] J. L. Bernal, L. Verde, and A. G. Riess, The trouble with H_0, J. Cosmol. Astropart. Phys. 10 (2016) 019.
[56] K. Aylor, M. Joy, L. Knox, M. Millea, S. Raghunathan, and W. L. Kimmy Wu, Sounds discordant: Classical distance ladder & ΛCDM-based determinations of the cosmological sound horizon, Astrophys. J. **874**, 4 (2019).
[57] V. Poulin, T. L. Smith, D. Grin, T. Karwal, and M. Kamionkowski, Cosmological implications of ultralight axionlike fields, Phys. Rev. D **98**, 083525 (2018).
[58] V. Poulin, T. L. Smith, T. Karwal, and M. Kamionkowski, Early Dark Energy Can Resolve the Hubble Tension, Phys. Rev. Lett. **122**, 221301 (2019).
[59] P. Agrawal, F.-Y. Cyr-Racine, D. Pinner, and L. Randall, Rock 'n' Roll solutions to the Hubble tension, arXiv:1904.01016.
[60] C. M. Will, The confrontation between general relativity and experiment, Living Rev. Relativity **17**, 4 (2014).
[61] B. Bertotti, L. Iess, and P. Tortora, A test of general relativity using radio links with the Cassini spacecraft, Nature (London) **425**, 374 (2003).
[62] C. Wetterich, Cosmologies with variable Newton's "constant", Nucl. Phys. **B302**, 645 (1988).
[63] D. Paoletti, M. Braglia, F. Finelli, M. Ballardini, and C. Umiltà, Isocurvature fluctuations in the effective Newton's constant, Phys. Dark Universe **25**, 100307 (2019).
[64] S. M. Du, Scalar stochastic gravitational-wave background in Brans-Dicke theory of gravity, Phys. Rev. D **99**, 044057 (2019).
[65] B. P. Abbott *et al.* (LIGO Scientific and Virgo Collaborations), Tests of General Relativity with GW170817, Phys. Rev. Lett. **123**, 011102 (2019).
[66] Y. Akrami *et al.* (Planck Collaboration), Planck 2018 results. I. Overview and the cosmological legacy of Planck, arXiv:1807.06205.
[67] Y. Akrami *et al.* (Planck Collaboration), Planck 2018 results. II. Low frequency instrument data processing, arXiv:1807.06206.
[68] N. Aghanim *et al.* (Planck Collaboration), Planck 2018 results. III. High frequency instrument data processing and frequency maps, arXiv:1807.06207.